Comparative Topographical Analysis of Choroidal Microvascular Dropout Between Glaucoma and Nonarteritic Anterior Ischemic Optic Neuropathy

Eun Jung Lee, Hyun Joo Kee, Kyung-Ah Park, Jong Chul Han, and Changwon Kee

Department of Ophthalmology, Samsung Medical Center, Sungkyunkwan University School of Medicine, Seoul, Korea

Correspondence: Changwon Kee, Department of Ophthalmology, Samsung Medical Center, Sungkyunkwan University School of Medicine, 81 Irwon-ro, Gangnam-gu, Seoul 06351, Korea; ckee@skku.edu.

Received: July 7, 2021
Accepted: October 5, 2021
Published: October 27, 2021

Citation: Lee EJ, Kee HJ, Park KA, Han JC, Kee C. Comparative topographical analysis of choroidal microvascular dropout between glaucoma and nonarteritic anterior ischemic optic neuropathy. *Invest Ophthalmol Vis Sci.* 2021;62(13):27. https://doi.org/10.1167/iovs.62.13.27

Purpose. To identify the presence of choroidal microvascular dropout (MvD) in nonarteritic anterior ischemic optic neuropathy (NAION) eyes and to characterize the topographical distribution for the mechanistic interpretation of MvD development.

Methods. We performed optical coherence tomography angiography on 47 open-angle glaucoma (OAG) and 19 NAION eyes with β-zone peripapillary atrophy (βPPA). We recorded the presence of MvD and compared between the peripapillary topographical measures of MvD, retinal nerve fiber layer (RNFL) defect, and βPPA in angular width and location.

Results. MvD was present in both diseases, marginally more frequently in NAION eyes (19/19, 100.0%) than in OAG eyes (38/47, 80.6%, $P = 0.050$), without a discernable difference in appearance. NAION eyes also showed wider MvD and RNFL defects compared to OAG eyes (both $P < 0.001$). In topographical measurements, the distribution of MvD showed a strong correspondence to superimposition areas of βPPA and RNFL defects, more distinctly than to RNFL defects (all $P < 0.001$). The outline of superimposition area also remarkably resembled the MvD area.

Conclusions. MvD was present in both the OAG and NAION groups. The βPPA-RNFL defect superimposition area topographically and morphologically matched MvD. Further investigations are needed to elucidate the role of RNFL defects in the pathogenesis of MvD and the clinical significance.

Keywords: glaucoma, microvascular dropout, choroid, peripapillary atrophy

Optical coherence tomography (OCT) angiography (OCTA) has revealed choroidal microvascular dropout (MvD) in the peripapillary area of some glaucomatous eyes.[1,2] MvD is defined as a loss of the microvasculature located within the deep retinal layer of the β-zone peripapillary atrophy (βPPA).[2] Regarding the close relationship to glaucoma progression,[1–7] MvD has been considered a sign of decreased ocular perfusion in the optic nerve head (ONH).[4,7–10]

However, the clinical significance of MvD remains to be elucidated. MvD may develop secondarily in response to retinal nerve fiber layer (RNFL) defect[11] or may precede the axonal damage in the ONH in relation to ischemia.[4,7–10] The cases of nonglaucomatous MvD[3,11,12] and the spatial association between MvD and RNFL defect[9,13,14] have led researchers to consider MvD as secondary to RNFL defect.

In this regard, the presence of MvD in nonarteritic anterior ischemic optic neuropathy (NAION) is of particular clinical relevance because NAION is an optic neuropathy that shares a similar pattern of RNFL loss with glaucoma but with different etiology. MvD in NAION shows that MvD is not specific to glaucomatous RNFL damage. In addition, the ischemic role of MvD in glaucoma originates from the ischemic theory of glaucoma, in which the peripapillary choroid contributes to the blood supply to the ONH.[15,16] Thus, the MvD in NAION indicates that we may consider pathways other than the "choroid-to-RNFL" sequence adopted in glaucoma.

In this study, we examined the eyes with NAION and open-angle glaucoma (OAG) for the presence of MvD. We also characterized topographic features of MvD, RNFL defect, and βPPA to suggest a new structural interpretation of MvD development.

Methods

This was a cross-sectional study. The subjects consisted of patients with OAG and NAION who visited the Samsung Medical Center (Seoul, South Korea) between December 2015 and March 2021. This study followed all the guidelines for experimental investigation in human subjects and was approved by the Samsung Medical Center Institutional Review Board and adhered to the tenets of the Declaration of Helsinki.

The inclusion criteria of OAG included (1) the presence of glaucomatous optic disc changes, such as increased cupping, diffuse or focal neural rim thinning, disc hemorrhage, or RNFL defect; (2) an open angle on gonioscopic examination; and (3) glaucomatous visual field (VF) defects detected by more than one reliable test for at least two of the following

three criteria: (1) a cluster of three points with a probability of less than 5% on the pattern deviation map in at least one hemifield, including at least one point with a probability of less than 1% or a cluster of two points with a probability of less than 1%; (2) a glaucoma hemifield test result outside normal limits; and (3) a pattern standard deviation (PSD) of 95% outside the normal limits. Reliable VF analysis was defined as a false-negative rate of <15%, a false-positive rate of <15%, and a fixation loss of <20%.

The inclusion criteria of NAION included (1) development of painless vision loss within 30 days of documented optic disc swelling confirmed by an ophthalmologist, (2) patient age between 40 and 85 years, (3) VF loss consistent with NAION, and (4) a relative afferent pupillary defect, unless the fellow eye affected in the past or both eyes were simultaneously affected with similar intensity. We only included chronic NAION eyes with a follow-up of at least 6 months after the acute phase. The exclusion criteria of NAION included (1) history or signs of any other intraocular, orbital, or intracranial disease; (2) history of ocular trauma; (3) other types of optic neuropathy suggested by ocular manifestation, history, or blood tests, including arteritic anterior ischemic optic neuropathy (AION), inflammatory optic neuritis, or glaucoma, such as glaucomatous optic disc change or increased IOP; and (4) medication known to affect visual function (e.g., ethambutol, digoxin, and vigabatrin) or to cause miosis (e.g., opioids).

In both diseases, we excluded eyes without βPPA; we only included the eyes with confirmed βPPA on fundus photograph and OCT. Eyes with media opacities and systemic or ocular diseases that could affect the VF test and OCTA were excluded.

Each participant underwent a comprehensive ophthalmic examination, including slit-lamp biomicroscopy, manifest refraction, tonometry, dilated stereoscopic examination of the ONH, color and red-free fundus photography (TRC-50DX model; Topcon Medical System, Inc., Oakland, NJ, USA), automated perimetry using a central 24-2 or 30-2 Humphrey field analyzer (HFA model 640; Humphrey Instruments, Inc., San Leandro, CA, USA) with the Swedish interactive threshold algorithm standard, spectral-domain OCT with Cirrus HD-OCT (Carl Zeiss Meditec, Dublin, CA, USA), and swept-source OCTA (DRI OCT Triton; Topcon, Tokyo, Japan).

We prescribed IOP-lowering eye drops, depending on the judgment of the treating clinician for each patient. We used combinations or choices of commercially available prostaglandin analogues, β-blockers, carbonic anhydrase inhibitors, and α-2 adrenergic agonists, with subsequent additional medication based on clinical judgment. Patients with primary OAG were offered laser trabeculoplasty or glaucoma surgery when medical treatment failed.

Assessment of the MvD: Presence, Angular Width, and Location

The optic nerve and parapapillary area were imaged using a commercially available swept-source OCTA device (DRI OCT Triton; Topcon) following a previously published method.[17] Briefly, the deep-layer microvasculature in the peripapillary area was evaluated on the en face images of the deep layer by automated layer segmentation in the OCT instrument software, extending from the retinal pigment epithelium (RPE) to 390 µm below Bruch's membrane. MvD was determined when the circumferential width was more than two times greater than the width of the visible juxtapapillary microvessels.[1]

We marked the boundary of the MvD using the tool provided by the OCTA viewer software (IMAGEnet 6; Topcon). The area covered by the large retinal vessels was included as part of the MvD if the dropout extended beyond the vessels. The en face OCT image with marked MvD was then manually superimposed on the fundus photograph using a commercial software (Photoshop CC; Adobe Systems, Mountain View, CA, USA; Fig. 1). The angular width of MvD was measured based on the inner margin, and the median angular location of MvD was measured from the fovea–ONH center axis following a previous report.[17] We also measured the area of the optic disc and peripapillary atrophy (PPA) using the same program. The margin of the PPA area devoid of the RPE was determined by comparing the coaligned OCT images.

Assessment of RNFL Defect and βPPA–RNFL Defect Superimposition

The boundary of the RNFL defect was determined using color and red-free photographs. When the boundaries were unclear, the OCT RNFL thickness deviation map was also used. We defined βPPA–RNFL defect superimposition as the peripapillary area confined to the βPPA, where the wedge-shaped RNFL overlapped onto the βPPA. The width and location of the RNFL defect and βPPA–RNFL defect superimposition area were measured using the same method as for MvD. Measurements were performed using ImageJ (National Institutes of Health, Bethesda, MD, USA).

Clock-Hour RNFL Thickness and Location of MvD, βPPA, RNFL Defect, and βPPA–RNFL Defect Superimposition

We obtained the 12 clock-hour RNFL thicknesses from Cirrus HD-OCT. The frequency of MvD, RNFL defect, and βPPA–RNFL defect superimposition at each clock-hour location was recorded after synchronizing the clock-hour meridian reference line in the Cirrus HD-OCT with fundus photographs. We superimposed the infrared photograph with the peripapillary RNFL thickness scan circle provided in Cirrus HD-OCT. We counted the corresponding clock hour as having MvD or RNFL defects when the involvement occupied over more than half an hour.

Data Analysis

The clock-hour distributions of the investigated parameters are shown in the radar charts. Quantitatively, we correlated the width/location of MvD, RNFL defect, βPPA, and βPPA–RNFL defect superimposition using Spearman's correlation analysis. The measured topographic parameters were also compared across subgroups of MvD (+) OAG, MvD (−) OAG, and NAION. To identify potential differences in baseline characteristics between the two disease groups, we compared patients' age, sex, history of diabetes and hypertension, refractive error, IOP, VF indices, and

Investigative Ophthalmology & Visual Science

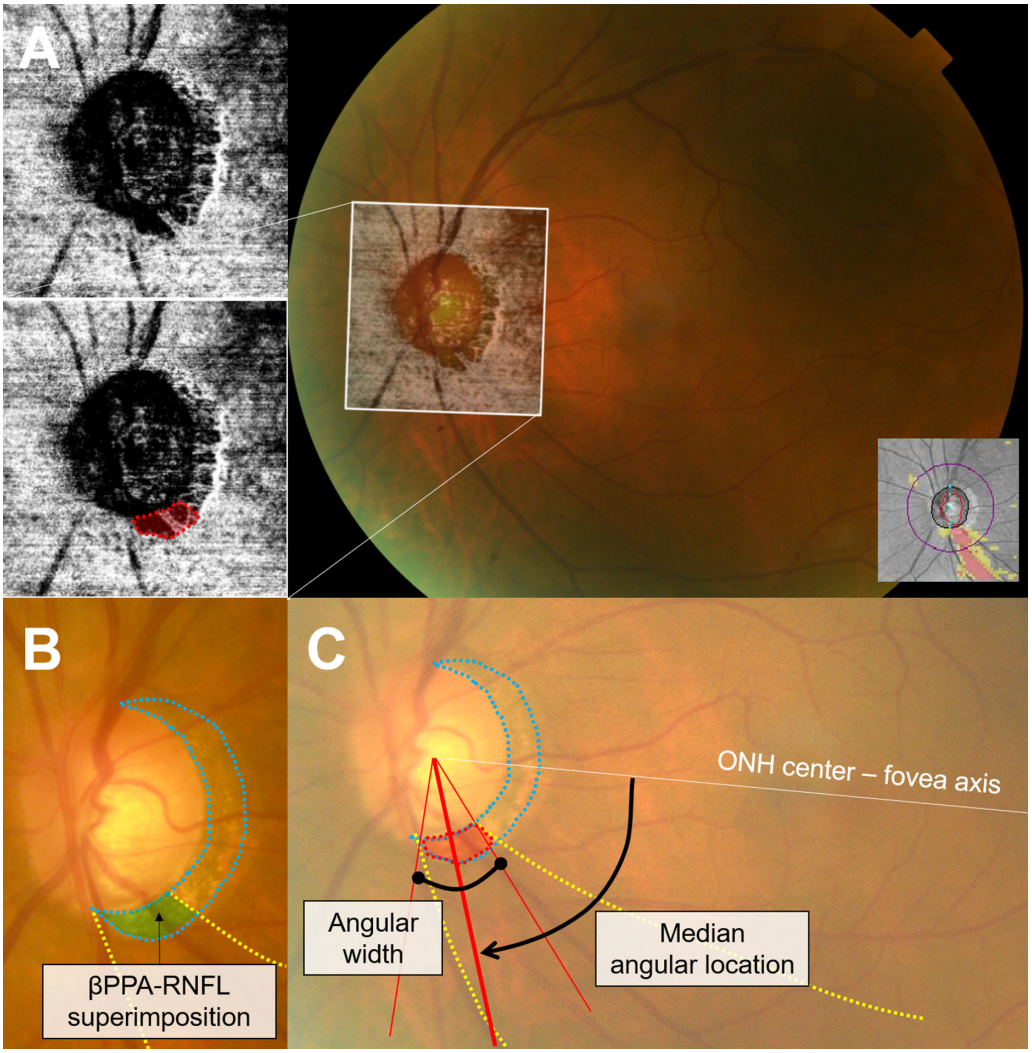

Figure 1. Topographic measurement of MvD, RNFL defect, and βPPA–RNFL defect superimposition. (**A**) A superimposed image (*right*) constructed using an OCTA en face image of the choroidal layer (*left upper*) and a color fundus photograph. *Red dotted line* marks the boundary of MvD (*left lower*). (**B**) The definition of βPPA–RNFL defect superimposition area (*green shade*). (**C**) The angular width (between *thin red lines*) and median angular location of the MvD (*red shade*). The ONH center–fovea axis was used as a reference line. *Yellow dotted line* indicates boundaries of the RNFL defect and *blue dotted line* indicates boundaries of the βPPA.

global/clock-hour RNFL thickness. Mean deviation (MD) of −31.43 dB and PSD of 1.81 were used as the values for no light perception in the two eyes.[18] Categorical variables were compared using Fisher's exact test. Regarding continuous variables, we used an independent *t*-test to compare the OAG and NAION groups, and one-way ANOVA and ad hoc analysis using Tukey's method were used to compare across the subgroups. One eye per patient was used, that is, the randomly selected eye in the OAG group and the affected eye in the NAION group. In the case of more than one MvD or RNFL defect, the parameters of each defect were recorded separately.

Two independent readers (EJL and HJK) who were blinded to the clinical information of the patients evaluated the presence of MvD, and discrepancies were resolved by consensus. The interobserver agreement of the presence of MvD and MvD width/location was determined using the κ coefficient and intraclass correlation coefficient (ICC), respectively. All statistical analyses were performed using SPSS statistical software (version 25.0; SPSS, Chicago, IL, USA). Statistical significance was set at $P < 0.05$.

Results

Among the initial 68 patients, we excluded 3 patients with OAG who had a history of retinal vein occlusion, 1 patient with NAION who had suspicious arteritic AION, and 4 patients with NAION and 3 patients with OAG who had poor-quality OCTA images.

Presence of MvD

Finally, 38 eyes of 38 patients in the OAG group and 19 eyes of 19 patients in the NAION group were evaluated. MvD was present in 38 of 47 glaucomatous eyes and in the 19 NAION eyes (38/47 vs. 19/19, $P = 0.050$). The interobserver agreement for the detection of MvD was excellent ($\kappa = 0.886$).

Investigative Ophthalmology & Visual Science

Baseline Clinical Characteristics of the OAG and NAION Groups

Table 1 shows the clinical characteristics of the patients. The NAION group had significantly worse VF MD and PSD than the OAG group, while the global RNFL thickness was comparable ($P = 0.017$, 0.010, and 0.247, respectively). The disc and βPPA area were also comparable. The NAION group showed significantly thinner RNFL in 11, 12, 1, and 2 o' clock (o/c) and significantly thicker RNFL in 5 and 6 o/c than the OAG group. Other parameters, including refractive error and IOP, were comparable between the groups.

The OAG group comprised 38 patients with normal-tension glaucoma (NTG) and 9 patients with primary OAG who had been treated for 6.3 ± 6.0 years. All patients were medically treated, except for three patients with primary OAG; two patients received trabeculectomy and one patient received selective laser trabeculoplasty. The number of medications was 2.0 ± 1.1 (1–4) at the time of OCTA examination.

The General Appearance of MvD

In all eyes, the MvD boundary coincided with βPPA to the radial extent, as previously reported.[1,9] In other words, we did not observe MvD outside the area of βPPA.

The lateral border of MvD was often delineated by medium-sized and large-sized vessels, as defined in this study. Therefore, the MvD border was frequently affected not only by the vascular dropout itself but also by the presence of projection artifacts of retinal vessels, large choroidal vessels, or vessel crowding.

In most cases, the general shape and extent of MvD closely resembled the area of RNFL defect and βPPA superimposition. In some cases, there were discrepancies; mildly wider or narrower MvD was seen compared to the RNFL defect area. Overall, the general appearance was indistinguishable between the OAG and NAION.

Location of MvD, RNFL Defect, and βPPA–RNFL Defect Superimposition

Figure 2A shows the RNFL thickness and the presence of MvD by clock hour. Figure 2B shows the radar charts demonstrating the spatial conformity between the MvD, RNFL defect, and βPPA–RNFL defect superimposition. MvD almost completely conformed to the direction of the βPPA–RNFL defect superimposition, invariably in both diseases. The angular width of MvD was larger in NAION compared with OAG.

Strength of Topographical Correlation Between MvD, RNFL Defect, and βPPA–RNFL Defect Superimposition

We observed excellent interobserver agreement for measuring the width (ICC = 0.991) and angular location (ICC = 0.993) of MvD in the entire study group.

Table 1. Characteristics of the OAG and NAION Eyes With MvD

Characteristic	OAG Group	NAION Group	*P* Value*
Number of eyes	44	19	NA
Sex (female/male), *n*	24/23	7/12	0.415
Age at OCTA, y	61.1 ± 10.7	63.3 ± 9.9	0.451
Refractive error, diopters	−1.74 ± 2.38	−0.44 ± 2.37	0.067
Intraocular pressure, mm Hg	14.1 ± 3.0	14.7 ± 2.5	0.461
Diabetes mellitus, *n* (%)	3 (6.4)	8 (42.1)	**0.001**
Hypertension, *n* (%)	14 (29.8)	5 (26.3)	1.000
VF MD, dB	−11.85 ± 6.72 (−28.22 to −2.61)	−18.31 ± 10.10 (−31.43 to −3.0)	**0.017**
VF PSD, dB	12.57 ± 6.36 (4.08 to 45.68)	8.30 ± 4.46 (1.82 to 15.38)	**0.010**
RNFL thickness,† µm			
Global	70.4 ± 11.3	67.0 ± 9.1	0.247
Superior	89.8 ± 22.4	67.1 ± 12.7	**<0.001**
Temporal	59.1 ± 11.4	55.1 ± 9.3	0.174
Inferior	66.9 ± 13.7	83.9 ± 20.3	**0.003**
Nasal	62.5 ± 10.9	61.6 ± 8.2	0.757
12 o/c (superior)	91.7 ± 28.9	65.2 ± 18.6	**<0.001**
1 o/c	89.4 ± 29.9	66.2 ± 13.8	**<0.001**
2 o/c	69.9 ± 17.0	51.8 ± 14.9	**<0.001**
3 o/c (temporal)	53.4 ± 11.0	51.3 ± 9.6	0.473
4 o/c	54.0 ± 13.2	57.3 ± 13.1	0.359
5 o/c	60.6 ± 15.9	90.0 ± 35.8	**0.002**
6 o/c (inferior)	65.8 ± 17.9	86.2 ± 22.3	**<0.001**
7 o/c	75.5 ± 18.3	75.4 ± 16.8	0.973
8 o/c	58.3 ± 14.4	60.7 ± 9.0	0.510
9 o/c (nasal)	57.4 ± 8.9	59.7 ± 7.1	0.334
10 o/c	72.2 ± 15.9	65.7 ± 11.5	0.112
11 o/c	87.8 ± 24.2	69.8 ± 19.4	**0.005**
Disc size, mm^2	2.262 ± 0.490	2.143 ± 0.313	0.247
PPA size, mm^2	1.008 ± 0.649	0.889 ± 0.652	0.503
Eyes with MvD, *n* (%)	38 (80.9)	19 (100.0)	**0.050**

Values are presented as mean ± SD unless otherwise indicated. Boldface indicates statistical significance. NA, not applicable.
* Independent *t*-test for continuous variables and Fisher's exact test for categorical variables.
† Right eye data were converted into the left eye format for clock-hour thickness.

Investigative Ophthalmology & Visual Science

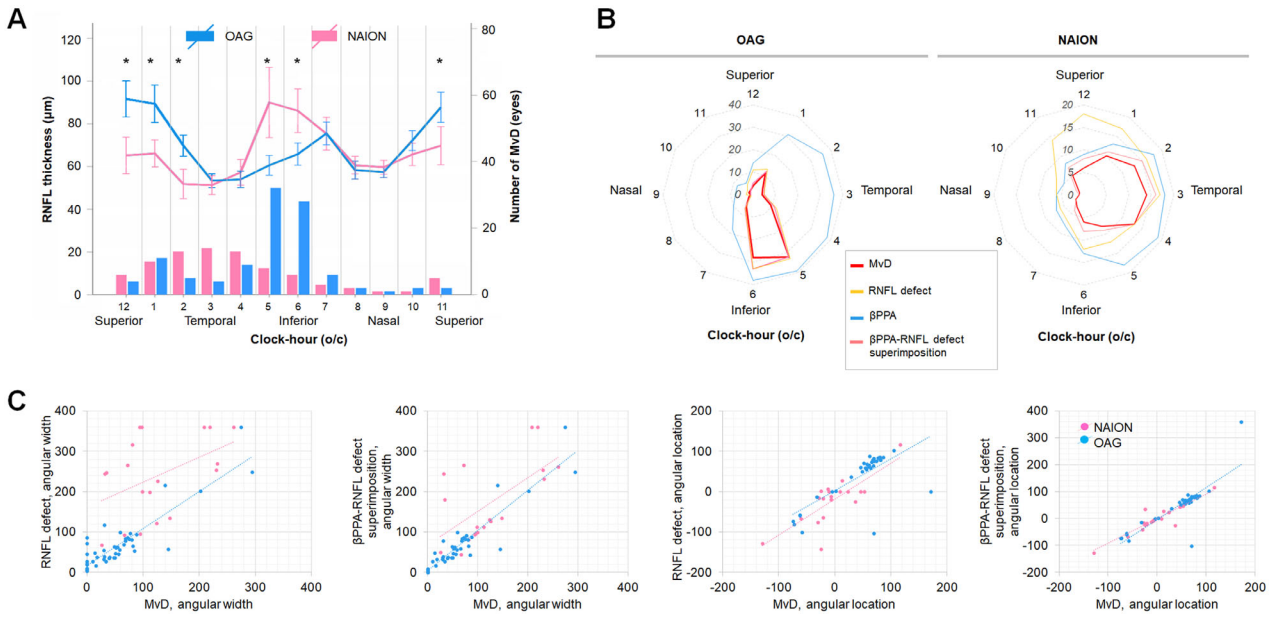

Figure 2. Topographic distribution and the correspondence of MvD, RNFL defect, and βPPA–RNFL defect. (**A**) Clock-hour profile of RNFL thickness (*lines*) and frequency of MvD (*bars*) in OAG (*blue*) and NAION (*pink*). *Asterisks* indicate significant differences in RNFL thickness between the NAION and OAG groups. *Error bars* indicate ±2 standard error. (**B**) Radar charts showing that MvD (*red line*) highly matches the distribution of βPPA–RNFL defect superimposition (*pink line*) in both diseases more strongly than RNFL defect (*yellow line*) and βPPA (*blue line*). Right eye data were converted into the left eye format for the clock-hour thickness. (**C**) Graphs showing the correlations between MvD, RNFL defect, and βPPA–RNFL defect superimposition. All relationships are statistically significant in both the NAION and OAG groups. Note the stronger association for βPPA–RNFL defect superimposition than for RNFL defect alone. *Blue* indicates OAG and *pink* indicates NAION.

Table 2. Topographical Correlation Between MvD, βPPA, and RNFL Defect

	Angular Width		Angular Location	
Characteristic	**RNFL Defect**	**βPPA–RNFL Defect Superimposition**	**RNFL Defect**	**βPPA–RNFL Defect Superimposition**
MvD, angular width				
Total group	0.830 (<0.001)	0.856 (<0.001)		
OAG	0.867 (<0.001)	0.897 (<0.001)		
NAION	0.400 (0.090)	0.543 (0.016)		
MvD, angular location				
Total group			0.757 (<0.001)	0.808 (<0.001)
OAG			0.730 (<0.001)	0.844 (<0.001)
NAION			0.608 (0.006)	0.749 (<0.001)

Data are presented as Spearman's correlation coefficient (*P* value).

Figure 2C and Table 2 show the strong correlation between the angular width and location of the MvD, RNFL defect, and βPPA–RNFL defect superimposition in the entire study group (all $P < 0.001$), in concert with previous reports.[9,13,14] Notably, the strength of the correlation was consistently higher in the βPPA–RNFL defect superimposition than in the RNFL defect alone; in NAION, the correlation between the angular width of MvD and RNFL defects was insignificant ($P = 0.090$), while the βPPA–RNFL defect superimposition successfully demonstrated a significant relationship ($P = 0.016$).

In addition, in terms of the strength of correlation between the angular widths, NAION eyes showed a weaker correlation than POAG eyes (coefficient 0.400 and 0.543 vs. 0.854 and 0.914, respectively).

Quantitative Comparison of RNFL Defect and βPPA–RNFL Defect Superimposition in the Subgroups of MvD (+) OAG, MvD (−) OAG, and NAION

Table 3 compares the topographical measurements of RNFL defect and βPPA–RNFL defect superimposition of the subgroups. MD was significantly worse in the NAION group than in two OAG subgroups ($P = 0.036$ and 0.003), but there was no difference between OAG subgroups ($P = 0.167$). Global RNFL thickness was significantly different between the MvD (−) OAG and NAION groups ($P = 0.006$) and between the MvD (+) OAG and MvD (−) OAG groups ($P = 0.006$) but not between NAION and MvD (+) OAG groups ($P = 0.915$).

Table 3. Comparison of MvD, PPA, and RNFL Defect Topography Among the Subgroups

Parameters	MvD (+) OAG (A), Mean ± SD	MvD (−) OAG (B), Mean ± SD	NAION (C), Mean ± SD	*P* Value*	Ad Hoc		
					A–B	B–C	A–C
Number of eyes	38	9	19	NA	NA	NA	NA
Age, y	62.7 ± 10.4	54.3 ± 9.6	63.3 ± 9.9	0.070	0.075	0.084	0.980
VF MD, dB	−12.85 ± 6.99	−7.62 ± 2.98	−18.31 ± 10.10	**0.003**	0.167	**0.003**	**0.036**
VF PSD, dB	12.78 ± 6.77	11.66 ± 4.45	8.30 ± 4.46	**0.032**	0.865	0.347	**0.024**
Global RNFL thickness, µm	68.1 ± 9.7	80.0 ± 12.7	67.0 ± 9.1	**0.004**	**0.006**	**0.006**	0.915
Refractive error, diopters	−1.77 ± 2.46	−1.66 ± 2.19	−0.44 ± 2.37	0.188	0.992	0.447	0.173
Intraocular pressure, mm Hg	14.0 ± 3.0	14.7 ± 3.2	14.7 ± 3.0	0.638	0.821	0.999	0.664
Disc size, mm^2	2.279 ± 0.498	2.191 ± 0.473	2.143 ± 0.313	0.547	0.859	0.963	0.536
PPA size, mm^2	1.079 ± 0.678	0.710 ± 0.421	0.889 ± 0.652	0.246	0.275	0.770	0.548
PPA circumferential width, deg	238.0 ± 88.1	189.9 ± 61.6	220.9 ± 93.2	0.315	0.299	0.652	0.763
Angular width, total, deg							
MvD	85.2 ± 61.1	0.0 ± 0.0	126.0 ± 70.8	**<0.001**	**0.001**	**<0.001**	**0.049**
RNFL defect	104.5 ± 71.1	18.5 ± 21.1	240.4 ± 97.8	**<0.001**	**0.009**	**<0.001**	**<0.001**
PPA–RNFL defect superimposition	93.4 ± 67.9	6.9 ± 1.8	171.8 ± 96.9	**<0.001**	**0.006**	**<0.001**	**0.001**
Angular width, per each defect, deg							
MvD	57.8 ± 59.3	0.0 ± 0.0	114.0 ± 76.4	**<0.001**	**<0.001**	**<0.001**	**<0.001**
RNFL defect	70.9 ± 60.7	15.2 ± 20.1	228.4 ± 107.7	**<0.001**	0.052	**<0.001**	**<0.001**
PPA–RNFL defect superimposition	63.9 ± 63.3	5.5 ± 2.3	157.2 ± 101.6	**<0.001**	**<0.001**	**<0.001**	**<0.001**
Angular location, deg							
MvD	39.1 ± 57.9	NA	−7.1 ± 50.5	**0.003**	NA	NA	NA
RNFL defect	11.9 ± 74.0	30.4 ± 69.5	−25.9 ± 58.3	0.059	0.706	0.089	0.102
PPA–RNFL defect superimposition	23.4 ± 82.3	24.9 ± 70.0	−12.1 ± 53.5	0.170	0.998	0.385	0.162

Boldface indicates statistical significance. A positive sign was assigned to the angular locations in the inferior hemi-retina direction.
* One-way ANOVA and Tukey's method for ad hoc analysis.

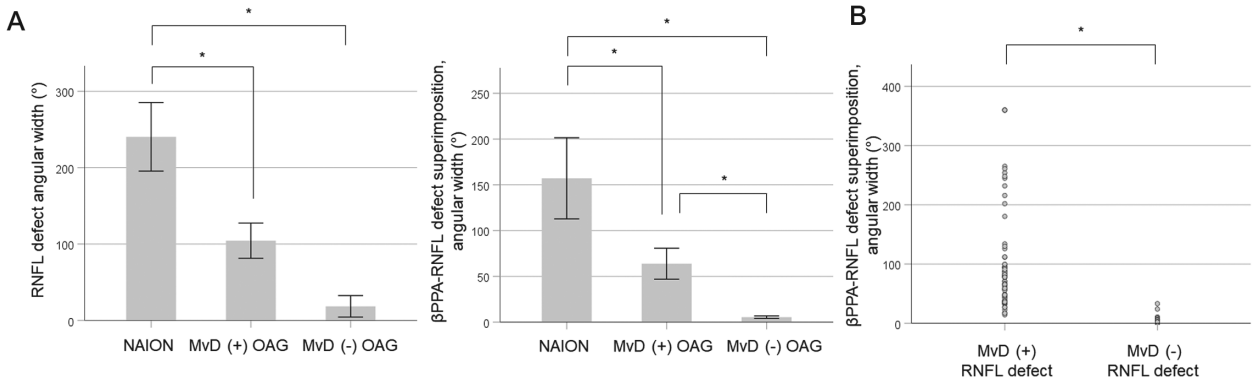

Figure 3. Quantitative comparison between MvD, RNFL defect, and βPPA–RNFL defect superimposition in the subgroups. (**A**) *Bar graphs* showing the angular width of RNFL defect and βPPA–RNFL defect superimposition in the NAION, MvD (+) OAG, and MvD (−) OAG. (**B**) Distribution of βPPA–RNFL defect in RNFL defects with and without MvD. The distribution is almost bisected with minimal overlap. *Error bars* indicate ±2 standard errors. *Asterisks* indicate significant differences between the subgroups.

The angular widths of the MvD, RNFL defect, and βPPA–RNFL defect superimposition differed significantly. The total MvD was significantly wider in the NAION group than in the MvD (+) OAG subgroup (mean 126.0° vs. 85.2°, $P = 0.049$). The widths of the total RNFL defect and βPPA–RNFL defect superimposition also decreased in the subgroups in the following order: NAION > MvD (+) OAG > and MvD (−) OAG (Fig. 3A). The angular location of MvD was more on the temporal side in the NAION compared with the glaucoma group (mean −7.1° vs. 39.1°, $P = 0.003$).

RNFL Defect and βPPA–RNFL Defect Superimposition by the Presence of MvD

In total, 12 OAG eyes with a total of 13 separate RNFL defects had no MvD. When counted per each RNFL defect, MvD corresponding to the RNFL defect was absent in 21 separate RNFL defects (20 in OAG eyes, 1 in NAION eye); 1 superotemporal RNFL defect in 1 NAION eye and 8 inferotemporal and 12 superotemporal RNFL defects in OAG eyes did not accompany MvD in the involved peripapillary location.

Investigative Ophthalmology & Visual Science

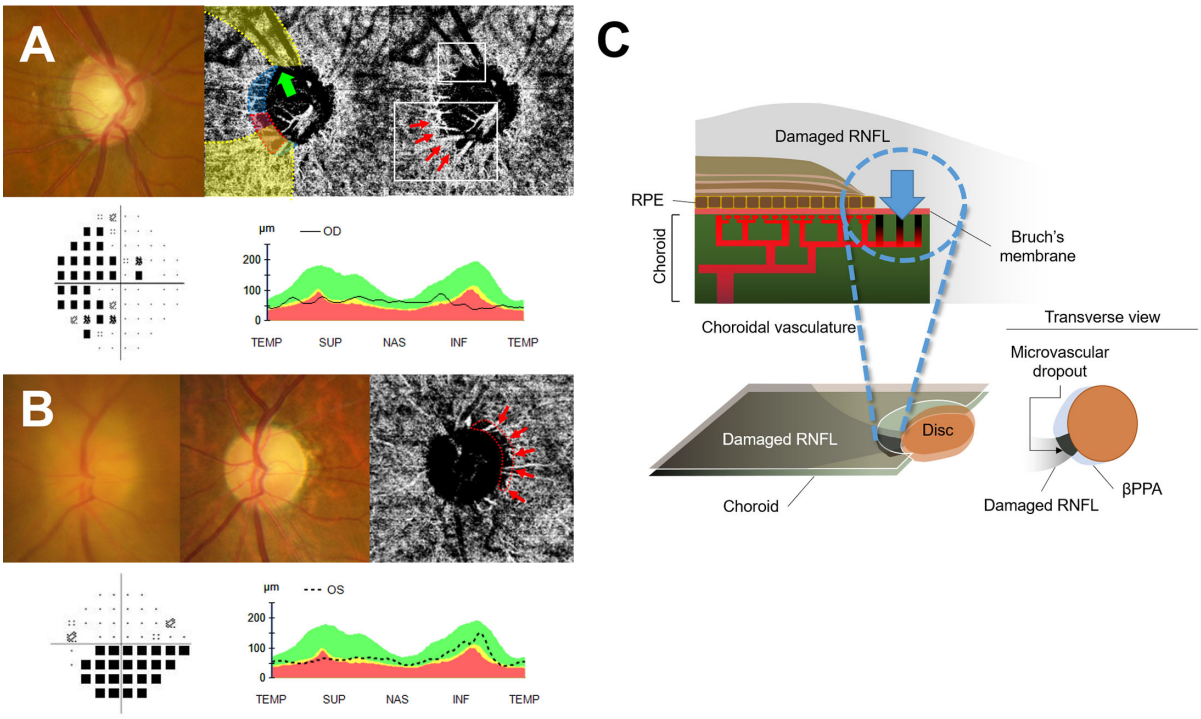

Figure 4. Representative cases of MvD in OAG and NAION. (**A**) An OAG case with MvD. The inferotemporal RNFL defect (*yellow shade*) with a significant superimposition onto the βPPA area (*blue shade*) that topographically matches MvD (*large white box*). Note that the superior RNFL defect, where the βPPA area narrowly avoids the RNFL defect, shows no MvD (*small white box*). (**B**) An NAION case with MvD in the superior and temporal peripapillary area. Note that MvD (surrounded by *red dotted line*) is restricted to the limited boundary of βPPA (*red arrows*) in both diseases. (**C**) The βPPA–RNFL defect superimposition area shows the most corresponding morphologic mimicry of MvD, explaining MvD topography better than the RNFL defect. The chances of RNFL-related MvD development will be greatest where RNFL and the peripapillary choroid meet with the shortest distance, at the βPPA. The precise match of MvD and βPPA–RNFL defect superimposition suggests an RNFL-related mechanism in MvD pathogenesis; currently, only topography-based assumptions are made, and further investigations would be necessary to directly explain the mechanism.

Per eye, the widths of RNFL defect and βPPA–RNFL defect superimposition were significantly smaller (18.5 ± 21.1° vs. 149.8 ± 102.9°, 6.9 ± 1.8° vs. 119.6 ± 86.3°, both $P < 0.001$), and the global RNFL thickness was significantly higher (80.0 ± 12.7° vs. 67.8 ± 9.5°, $P = 0.001$), in eyes without MvD than in eyes with MvD. All eyes without MvD had absent or minimal βPPA–RNFL superimposition (Supplementary Fig. S1).

Similarly, the width of βPPA–RNFL superimposition of MvD-free RNFL defects was extremely small (7.3 ± 7.8°, range 0–33.2°, 75th percentile: 8.2°). The distribution of the superimposition width was almost bisecting between RNFL defects with and without MvD (Fig. 3B); superimposition width over 20° was seen in only 2 cases, 1 case had 10.6° superimposition, and all the other 18 cases had superimposition less than 10°. In contrast, the RNFL defects had relatively wider distribution (mean 25.6 ± 34.4°, range 4.3–98.0°, 75th percentile: 40.1°), including RNFL defect of 71.1° width and the superimposition of 5.4° width, as well as RNFL defect of 86.0° width and the superimposition of 3.0° width.

Finally, Figure 4 shows representative cases and a diagram.

Discussion

To our knowledge, there has been no report on choroidal MvD in NAION. We present the first evidence of MvD in NAION where all NAION eyes with βPPA showed MvD. Our results corroborate the previous reports that MvD can be observed in optic neuropathies with RNFL loss other than glaucoma.[3,12]

The reports on nonglaucomatous MvD, our study, and the following studies suggest the RNFL-related development of MvD. Most of all, the spatial correspondence between RNFL defect and MvD in many studies was interpreted to indicate that MvD may be a finding associated with, and as a result of, the RNFL defect.[9,13,14] The proportional enlargement of MvD with glaucoma progression also indicates that MvD may not precede the chronic progressive damage in glaucoma.[4,5,19] Son et al.[13] reported that MvD is observed only at the location of the RNFL defect in eyes with hemiretina involvement and is usually found in the location of more severe RNFL defects in eyes with bi-hemiretinal involvement. Moreover, a recent case report indicated the precedence of RNFL defect to MvD, by showing the late development of MvD months after the RNFL defect had already been established.[11]

On the other hand, we acknowledge the fact that several studies also suggest that MvD may be an etiologic factor for glaucoma as a sign of decreased ocular perfusion.[5,7,8,20] MvD was accompanied by lower diastolic blood pressure[2] and early parafoveal scotoma,[21] and generalized choroidal vascularity loss was observed even in hemispheres without RNFL loss in eyes with MvD.[8] We do not oppose the role of the choroid in glaucoma[22–25] or the relationship between MvD and systemic vascular risk factors.[2,21] We cannot conclude the role of MvD on the health of anterior ONH from the

results of this study. Given the conflicting results, further investigations on a long-term longitudinal follow-up cohort should be performed to confirm this.

However, our study suggests a new perspective on MvD from the finding that MvD was exactly on and within the βPPA around the optic disc. The βPPA–RNFL defect superimposition successfully matched the location and extent of MvD; it was superior to the RNFL defect in explaining the presence, shape, location, and extent of MvD.

The topographic correspondence between MvD, RNFL defect, and βPPA may shed light on the pathogenesis and significance of MvD by suggesting the possibility of an RNFL defect that directly affects the choroid. The idea is largely based on the topography, supported by the structural correlation and the simplicity of explanation. Indeed, our findings do not directly explain the mechanism; rather, they provide clues through the topography. The chances of MvD development will be greatest when RNFL and the peripapillary choroid meet in the shortest distance at the βPPA. Our observations show that the outline of MvD exactly matches the βPPA area overlapping with RNFL damage. Another surprising coincidence is that the limits of the βPPA area coincide with the area devoid of RPE between RNFL and choroid,[26] which becomes particularly noticeable in a transverse view (Fig. 4). In the model, it would hardly be surprising that the βPPA–RNFL defect closely matches the MvD.

The structural association between RNFL defect and MvD as shown in Figure 4 may plainly explain (1) why the topography is related to the RNFL defect[9,13,14] and preconditioned by the presence of βPPA,[1,9,27] (2) why MvD and glaucomatous damage have a proportional relationship both cross-sectionally[1–6] and longitudinally,[3,5,7] and (3) why our study group showed such a high prevalence of MvD compared to other studies. The NAION eyes had 100% MvD and 100% PPA, while the eyes with compressive optic neuropathy had MvD in only 34.1% of eyes and PPA in only 68.2% of eyes.[3] Last, it is also useful to explain the absence of MvD in eyes with a wide RNFL defect by the absence of such superimposition.

The correspondence was consistent in OAG and NAION, with similar but partly different topographic distribution of RNFL loss. This finding corroborates the concordant relationship in compressive optic neuropathy, where RNFL thickness, retinal vascular density, and MvD are related.[3] Overall, the findings highlight the role of the RNFL defect on MvD, regardless of etiology.

The reasons for the relatively narrow MvD to RNFL defect and βPPA–RNFL defect superimposition in the NAION eye compared to the OAG eye are unclear. One possible candidate may be the extensive RNFL loss in NAION eyes, which was far beyond the extent of PPA; in OAG eyes, RNFL defect and PPA remained similar within the temporal side of the optic disc. This finding may further support the role of PPA in MvD, but other possible factors limiting the extent of MvD in NAION should also be investigated.

One might reasonably be concerned about whether MvDs are merely invisible, rather than nonexistent, outside the βPPA area. In fact, it has not been seriously questioned if MvD is truly absent outside βPPA. The concerns can be adequately addressed by acknowledging that OCTA is capable of detecting choroidal abnormalities under an intact RPE layer.[28–30] Therefore, it is unlikely that MvD abruptly stops at the margin of βPPA, not extending beyond the PPA with the segmental pattern of the choroidal vasculature.[31–33] It is more likely that MvD would exist only to the extent of PPA. Our explanation can be useful for addressing this issue, as well as explaining why MvD is limited by the boundaries of βPPA. In fact, the importance of PPAs, in relation to RNFL defect or MvD, has been hardly recognized except in a few studies[1,9,27]; Lee et al.[21] considered that MvD associated with or attributable to PPA would be observed most likely at the location of the widest PPA. In the future, it may be worthwhile to further investigate the role of βPPA in MvD development.

In this regard, based on our findings and the early reports on MvD,[1,10,20] the presence of PPA may influence the detection of MvD. This is important because not all eyes have βPPA. In population-based studies, the prevalence of βPPA in normal eyes was generally 10% to 20%, sometimes rising up to 50%.[34–37] Therefore, we may preconsider the presence of PPA as a factor in MvD detection. MvD may be absent in some eyes, primarily because βPPA is absent.

Our results should be interpreted with caution. Although our explanation may provide a convenient description, it does not elucidate the mechanism. As briefly mentioned, in the βPPA area, the RPE layer is absent.[26] The acellular region may provide a condition distinct from the rest of the retina, allowing a local interaction between the RNFL and choroid. Indeed, such a condition may allow simultaneous bidirectional interaction. The current understanding suggests that choroidal ischemic insults to axons occur at the level of the ONH in both NAION and glaucoma[38–40]; the pathway from the choroid to the axons outside the ONH, at the peripapillary retina, however, may be a new topic for future research. This possibility remains to be tested through further investigations.

In the retina, OCTA-based dropout is thought to be secondary to RNFL damage of any etiology.[41–43] In the choroid, a different involvement pattern has been questioned.[44] Our hypothesis may conceptually connect the retina and the choroid.

This study has several limitations, including the small sample size; however, NAION is a rare disease, and recruiting eyes with PPA is more challenging. Another difficulty was the technical limitations of the OCTA. The projection artifacts of retinal vessels often impair the clear delineation of the MvD boundary. In some eyes, the MvD shape did not coincide completely with the superimposition area, occupying partly more or less area. We strictly excluded obscure dropout area to avoid false-positive inclusions, and such strict criteria may have resulted in erroneous estimations of MvD. However, this does not impair the primary purpose of this study. In addition, the severity of RNFL and VF loss was not comparable between the groups. Ideally, we should compare two groups with similar severity to identify differences, and thus, it is not appropriate to assume that NAION eyes are more likely to accompany MvD than OAG eyes. However, the diverse ranges of different RNFL defects and PPA extents were necessary for this study, providing important discriminatory cues for MvD detection. Last, our study was performed only on eyes with βPPA; however, it may be a more appropriate method for MvD, and recent studies were also performed on eyes with PPA.[2,8,10]

In conclusion, we observed MvD in both OAG and NAION eyes. MvD highly matched the βPPA–RNFL defect superimposition area by location and shape, invariably in both diseases. MvD may be the result of a local interaction of RNFL defect, βPPA, and the choroid in the peripapillary area. Further investigation is needed to clarify the mechanism and clinical significance.

Investigative Ophthalmology & Visual Science

Acknowledgments

Disclosure: **E.J. Lee**, None; **H.J. Kee**, None; **K.-A. Park**, None; **J.C. Han**, None; **C. Kee**, None

References

1. Lee EJ, Kim TW, Kim JA, Kim JA. Parapapillary deep-layer microvasculature dropout in primary open-angle glaucoma eyes with a parapapillary gamma-zone. *Invest Ophthalmol Vis Sci.* 2017;58:5673–5680.
2. Suh MH, Zangwill LM, Manalastas PI, et al. Deep retinal layer microvasculature dropout detected by the optical coherence tomography angiography in glaucoma. *Ophthalmology.* 2016;123:2509–2518.
3. Kim GN, Lee EJ, Kim TW. Microstructure of nonjuxtapapillary microvasculature dropout in healthy myopic eyes. *Invest Ophthalmol Vis Sci.* 2020;61:36.
4. Park HL, Kim JW, Park CK. Choroidal microvasculature dropout is associated with progressive retinal nerve fiber layer thinning in glaucoma with disc hemorrhage. *Ophthalmology.* 2018;125:1003–1013.
5. Kim JA, Lee EJ, Kim TW. Evaluation of parapapillary choroidal microvasculature dropout and progressive retinal nerve fiber layer thinning in patients with glaucoma. *JAMA Ophthalmol.* 2019;137:810–816.
6. Jo YH, Kwon J, Shon K, Jeong D, Kook MS. Greater severity of glaucomatous damage in eyes with than without choroidal microvasculature dropout in open-angle glaucoma. *Invest Ophthalmol Vis Sci.* 2019;60:901–912.
7. Lee KM, Kim M, Oh S, Kim SH. Hemisphere opposite to vascular trunk deviation is earlier affected by glaucomatous damage in myopic high-tension glaucoma. *PLoS One.* 2020;15:e0233270.
8. Jo YH, Shin JW, Song MK, Won HJ, Kook MS. Choroidal microvasculature dropout is associated with generalized choroidal vessel loss within the beta-parapapillary atrophy in glaucoma. *Am J Ophthalmol.* 2020;215:37–48.
9. Han JC, Lee EJ, Kim SB, Kee C. The characteristics of deep optic nerve head morphology in myopic normal tension glaucoma. *Invest Ophthalmol Vis Sci.* 2017;58:2695–2704.
10. Suh MH, Zangwill LM, Manalastas PIC, et al. Deep-layer microvasculature dropout by optical coherence tomography angiography and microstructure of parapapillary atrophy. *Invest Ophthalmol Vis Sci.* 2018;59:1995–2004.
11. Lee JS, Lee WJ, Lim HW, Seong M. Progression of parapapillary choroidal microvascular dropout after disc hemorrhage in glaucoma patients: 2 case reports. *J Glaucoma.* 2021;30:e8–e12.
12. Lee EJ, Kim JA, Kim TW, Kim H, Yang HK, Hwang JM. Glaucoma-like parapapillary choroidal microvasculature dropout in patients with compressive optic neuropathy. *Ophthalmology.* 2020;127(12):1652–1662.
13. Son KY, Han JC, Kee C. Parapapillary deep-layer microvasculature dropout is only found near the retinal nerve fibre layer defect location in open-angle glaucoma [published online March 19, 2021]. *Acta Ophthalmol.*
14. Kim CY, Lee EJ, Kim JA, Kim H, Kim TW. Progressive retinal nerve fibre layer thinning and choroidal microvasculature dropout at the location of disc haemorrhage in glaucoma. *Br J Ophthalmol.* 2021;105:674–680.
15. Anderson DR, Braverman S. Reevaluation of the optic disk vasculature. *Am J Ophthalmol.* 1976;82:165–174.
16. Lieberman MF, Maumenee AE, Green WR. Histologic studies of the vasculature of the anterior optic nerve. *Am J Ophthalmol.* 1976;82:405–423.
17. Han JC, Choi JH, Park DY, Lee EJ, Kee C. Border tissue morphology is spatially associated with focal lamina cribrosa defect and deep-layer microvasculature dropout in open-angle glaucoma. *Am J Ophthalmol.* 2019;203:89–102.
18. Blumenthal EZ, Sapir-Pichhadze R. Misleading statistical calculations in far-advanced glaucomatous visual field loss. *Ophthalmology.* 2003;110:196–200.
19. Kwon J, Shin JW, Lee J, Kook MS. Choroidal microvasculature dropout is associated with parafoveal visual field defects in glaucoma. *Am J Ophthalmol.* 2018;188:141–154.
20. Lee EJ, Lee KM, Lee SH, Kim TW. Parapapillary choroidal microvasculature dropout in glaucoma: a comparison between optical coherence tomography angiography and indocyanine green angiography. *Ophthalmology.* 2017;124:1209–1217.
21. Lee EJ, Kim TW, Kim JA, Kim JA. Central visual field damage and parapapillary choroidal microvasculature dropout in primary open-angle glaucoma. *Ophthalmology.* 2018;125:588–596.
22. Flammer J, Orgul S, Costa VP, et al. The impact of ocular blood flow in glaucoma. *Prog Retin Eye Res.* 2002;21:359–393.
23. Hayreh SS. The blood supply of the optic nerve head and the evaluation of it—myth and reality. *Prog Retin Eye Res.* 2001;20:563–593.
24. Caprioli J, Coleman AL; Blood Flow in Glaucoma Discussion. Blood pressure, perfusion pressure, and glaucoma. *Am J Ophthalmol.* 2010;149:704–712.
25. Yamamoto T, Kitazawa Y. Vascular pathogenesis of normal-tension glaucoma: a possible pathogenetic factor, other than intraocular pressure, of glaucomatous optic neuropathy. *Prog Retin Eye Res.* 1998;17:127–143.
26. Curcio CA, Saunders PL, Younger PW, Malek G. Peripapillary chorioretinal atrophy: Bruch's membrane changes and photoreceptor loss. *Ophthalmology.* 2000;107:334–343.
27. Lee EJ, Kim TW, Lee SH, Kim JA. Underlying microstructure of parapapillary deep-layer capillary dropout identified by optical coherence tomography angiography. *Invest Ophthalmol Vis Sci.* 2017;58:1621–1627.
28. Nassisi M, Tepelus T, Nittala MG, Sadda SR. Choriocapillaris flow impairment predicts the development and enlargement of drusen. *Graefes Arch Clin Exp Ophthalmol.* 2019;257:2079–2085.
29. El Ameen A, Herbort CP, Jr. Serpiginous choroiditis imaged by optical coherence tomography angiography. *Retin Cases Brief Rep.* 2018;12:279–285.
30. Muller PL, Pfau M, Moller PT, et al. Choroidal flow signal in late-onset Stargardt disease and age-related macular degeneration: an OCT-angiography study. *Invest Ophthalmol Vis Sci.* 2018;59:AMD122–AMD131.
31. Mackenzie PJ, Cioffi GA. Vascular anatomy of the optic nerve head. *Can J Ophthalmol.* 2008;43:308–312.
32. Yoneya S, Tso MO. Angioarchitecture of the human choroid. *Arch Ophthalmol.* 1987;105:681–687.
33. Hayreh SS. Segmental nature of the choroidal vasculature. *Br J Ophthalmol.* 1975;59:631–648.
34. Jonas JB, Thomas R, George R, Berenshtein E, Muliyil J. Optic disc morphology in south India: the Vellore Eye Study. *Br J Ophthalmol.* 2003;87:189–196.
35. Wang Y, Xu L, Zhang L, Yang H, Ma Y, Jonas JB. Peripapillary atrophy in elderly Chinese in rural and urban Beijing. *Eye (Lond).* 2008;22:261–266.
36. Ramrattan RS, Wolfs RC, Jonas JB, Hofman A, de Jong PT. Determinants of optic disc characteristics in a general population: the Rotterdam Study. *Ophthalmology.* 1999;106:1588–1596.

Investigative Ophthalmology & Visual Science

37. Mataki N, Tomidokoro A, Araie M, Iwase A. Beta-peripapillary atrophy of the optic disc and its determinants in Japanese eyes: a population-based study. *Acta Ophthalmol.* 2018;96:e701–e706.
38. Weinreb RN, Aung T, Medeiros FA. The pathophysiology and treatment of glaucoma: a review. *JAMA.* 2014;311:1901–1911.
39. Quigley HA. The contribution of the sclera and lamina cribrosa to the pathogenesis of glaucoma: diagnostic and treatment implications. *Prog Brain Res.* 2015;220:59–86.
40. Hayreh SS. Ischemic optic neuropathy. *Prog Retin Eye Res.* 2009;28:34–62.
41. Fard MA, Suwan Y, Moghimi S, et al. Pattern of peripapillary capillary density loss in ischemic optic neuropathy compared to that in primary open-angle glaucoma. *PLoS One.* 2018;13:e0189237.
42. Fard MA, Yadegari S, Ghahvechian H, Moghimi S, Soltani-Moghaddam R, Subramanian PS. Optical coherence tomography angiography of a pale optic disc in demyelinating optic neuritis and ischemic optic neuropathy. *J Neuroophthalmol.* 2019;39:339–344.
43. Jia Y, Simonett JM, Wang J, et al. Wide-field OCT angiography investigation of the relationship between radial peripapillary capillary plexus density and nerve fiber layer thickness. *Invest Ophthalmol Vis Sci.* 2017;58:5188–5194.
44. Aghsaei Fard M, Salabati M, Mahmoudzadeh R, et al. Automated evaluation of parapapillary choroidal microvasculature in ischemic optic neuropathy and open angle glaucoma. *Invest Ophthalmol Vis Sci.* 2020;61:35.